International Journal of Nanomedicine

Dovepress
Taylor & Francis Group

Open Access Full Text Article

ORIGINAL RESEARCH

CD80 Antibody and MTX Co-Engineered Extracellular Vesicles Targets CD80$^+$ Macrophages to Suppress Inflammation and Alleviate Chronic Inflammatory Diseases

Jianhua Yang[1,*], Handan Zhang[2,*], Wenzhe Wang[1,*], Qiqi Yin[2,*], Xiaoning He[1], Dihao Tao[1], Hanzhe Wang[1], Wenhao Liu[1], Yiming Wang[1], Zhiwei Dong[3], Xin Chen[2], Bei Li[1]

[1]State Key Laboratory of Oral & Maxillofacial Reconstruction and Regeneration, National Clinical Research Center for Oral Diseases, Shaanxi International Joint Research Center for Oral Diseases, Center for Tissue Engineering, School of Stomatology, The Fourth Military Medical University, Xi'an, People's Republic of China; [2]Department of Chemical Engineering, Shaanxi Key Laboratory of Energy Chemical Process Intensification, Institute of Polymer Science in Chemical Engineering, School of Chemical Engineering and Technology, Xi'an Jiaotong University, Xi'an, 710049, People's Republic of China; [3]Department of Oral and Maxillofacial Surgery, College of Stomatology, Xi'an Jiaotong University, Xi'an, People's Republic of China

*These authors contributed equally to this work

Correspondence: Bei Li, State Key Laboratory of Oral & Maxillofacial Reconstruction and Regeneration, School of Stomatology, The Fourth Military Medical University, Xi'an, Shaanxi, 710032, People's Republic of China, Email libei2021@fmmu.edu.cn; Xin Chen, Institute of Polymer Science in Chemical Engineering, School of Chemical Engineering and Technology, Xi'an Jiao Tong University, Xi'an, Shaanxi, 710049, People's Republic of China, Email chenx2015@xjtu.edu.cn

Introduction: Aberrant interaction between innate immune and adaptive immune cells can disrupt tissue homeostasis, consequently triggering chronic inflammatory diseases such as rheumatoid arthritis (RA) and periodontitis (PD). Pro-inflammatory macrophages serve as critical mediators in the early immune response, constituting a major population of CD80$^+$ cells, while anti-inflammatory macrophages modulating inflammatory processes through the secretion of transforming growth factor-beta (TGF-β). This cytokine facilitates the differentiation of peripheral regulatory T cells (Tregs) and contributes to the establishment of immune tolerance. However, there are no definitive therapies to reshape the tissue homeostasis between innate immune and adaptive immune cells.

Methods: (1) anti-CD80-MTX-EVs was obtained by gradient centrifugation, which were characterized by TEM and DLS, and the associated membrane proteins were identified by Western Blot. (2) The mouse bone marrow-derived macrophages were co-cultured separately with EVs, anti-CD80-EVs, and anti-CD80-MTX-EVs in vitro, and the expression of CD80 on the macrophages surface as well as the proportion of Treg cell generation were detected. (3) EVs, anti-CD80-EVs and anti-CD80-MTX-EVs were injected into mice models of arthritis and periodontitis for treatment, the therapeutic effect was evaluated by the expressions of related cytokines, staining of HE, the proportion of CD80$^+$ macrophages and the phenotypic differentiation of T cells in the tissues.

Results: We successfully constructed engineered EVs (anti-CD80-MTX-EVs) targeting inflammatory macrophages for intracellular MTX delivering, which inducing the anti-inflammatory transformation while upregulating the expression of TGF-β of macrophages. Furthermore, our findings demonstrate that anti-CD80-MTX-EVs effectively reduce CD80$^+$ macrophage levels, promote Treg cell generation, and inhibit Th1 cell production in vivo.

Conclusion: In this study, the anti-CD80-MTX-Evs demonstrated significant therapeutic effects in both rheumatoid arthritis and periodontitis models through a triple mechanism: reducing CD80$^+$ macrophage population, enhancing Treg cell differentiation, and suppressing Th1 cell development. Overall, this study presents an innovative strategy for resolving inflammation within chronic inflammatory diseases.

Keywords: anti-CD80-MTX-EVs, macrophages, rheumatoid arthritis, periodontitis, immune tolerance, Treg cells

Received: 26 January 2025
Accepted: 13 May 2025
Published: 21 May 2025

Introduction

Unique groups of immune cells execute diverse functions, crucial for preserving tissue homeostasis through complex intercellular interactions. These interactions, mediated by a series of coordinated events, involve both innate and adaptive immune cells during inflammatory responses.[1–3] When inflammation fails to resolve, it can lead to chronic inflammatory diseases, such as RA and PD, which are characterized by severe bone damage and tissue destruction.[2,4] However, there are no definitive therapies to reshape the tissue homeostasis between innate and adaptive immune cells and resolve the chronic inflammatory diseases.

Among the innate immune responses, macrophages exhibit remarkable plasticity, adopting distinct functional states that can either promote or suppress inflammation.[5] Inflammatory macrophages play a critical role in initiating inflammation by releasing a variety of cytokines and chemokines, also enhancing the expression of costimulatory molecules like CD80 and CD86 to stimulate effector T cells.[6–8] Adaptive immune cells, in turn, actively engage in reciprocal communication with innate immune cells, further shaping the immune response and influencing the progression of inflammation. Regulatory T (Treg) cells, upon stimulation by transforming growth factor-β (TGF-β), synthesize interleukin-10 (IL-10), and various other cytokines. These cytokines play a crucial role in the immune system by maintaining tolerance to self-antigens, curbing excessive inflammation, and promoting tissue repair mechanisms.[9,10] Moreover, anti-inflammatory macrophages can regulate the inflammatory response by secreting TGF-β, which induce Tregs generation and immune tolerance.[11–13] Therefore, it is plausible to target and manipulate macrophages to induce Treg cells production and restore tissue homeostasis.

Extracellular vesicles (EVs) are increasingly recognized as a next-generation delivery system due to their numerous advantages, such as low immunogenicity,[14,15] inherent targeting capabilities,[16] extended circulation time, and the ability to cross biological barriers.[17,18] Recently, research has started to explore the role of EVs in modulating both innate and adaptive immune responses, demonstrating that engineered EVs can effectively suppress inflammation by influencing local macrophages and their interactions with T cells.[19,20] Nevertheless, additional research is necessary to comprehend and engineer EVs with specific targeting capabilities toward macrophages, as well as their ability to regulate interactions with T cells, particularly regulatory T cells (Tregs). Toward this end, the specific inflammatory macrophages, CD86 and CD80 positive macrophages were here characterized within collagen-induced arthritis (CIA) and ligature-induced PD mice models. Specific macrophages targeted EVs were engineered and introduced to regulate the interaction between macrophages and Tregs both in vitro and in vivo.

Methotrexate (MTX) is widely used in clinic to suppress inflammation, but which causes serious side effects.[21,22] In particular, MTX is capable of ameliorating RA disease activity by increasing Treg cell differentiation.[23] MTX-loaded EVs have been treated of lung cancer and glioblastoma without side effect.[24,25] Here, it is of significant interest to explore whether MTX-loaded extracellular vesicles (MTX-EVs) specifically targeted to macrophages could be developed to initiate synergistic immune responses between macrophages and regulatory T cells (Tregs). Such an approach could harness the unique properties of EVs to modulate immune interactions, potentially offering a novel therapeutic strategy for inflammatory diseases. We designed engineered EVs (anti-CD80-MTX-EVs) to target $CD80^+$ macrophages followed with intracellular MTX delivery to precisely regulate anti-inflammatory transformation of $CD80^+$ macrophages. Furthermore, anti-CD80-MTX-EVs were found to upregulate the expression of TGF-β and enhance the generation of Tregs. In vivo administration of anti-CD80-MTX-EVs effectively reduced the levels of $CD80^+$ macrophages, promoted Treg cell differentiation, and suppressed the production of Th1 cells. These effects collectively contributed to the significant alleviation of symptoms in both rheumatoid arthritis (RA) and periodontitis (PD) experimental models. This study highlights the potential of anti-CD80-MTX-EVs as a novel therapeutic approach to resolve inflammation in chronic inflammatory diseases, charting a course for the creation of innovative treatments.

Methods

Preparation of the DSPE-PEG-Anti-CD80

A total of 30 mg of DSPE-PEG-NH_2 (5000) was dissolved in the deionized water with 3 mL. Next, 4.6 mg of EDC, 1.8 mg of NHS, and 15 μL of CD80 antibody solution (1 μg/μL) were added, which was stirred for 3 hours at room

temperature. Subsequently, the mixture was shifted into a cellulose membrane dialysis cassette (molecular weight cutoff = 100,000) and dialyzed against 4.0 L of deionized water at room temperature overnight. The resulting DSPE-PEG-anti-CD80 solution was kept at 4°C for further applications. Detailed information regarding reagents were listed in the supporting information.

Isolation and Characterization of EVs

The human umbilical cord mesenchymal stem cells (hUCMSCs) were obtained with informed donor consent following healthy births from Tangdu Hospital. All processes were approved and supervised by the Ethics Committee of Tangdu Hospital of the Fourth Military Medical University and followed the Declaration of Helsinki, which incubated at 37°C with 5% CO_2 and 1% O_2. After a 48-hour incubation period, the cells were enzymatically detached using trypsin and subsequently seeded into a fresh culture plate. Next, the culture medium was augmented with methotrexate (MTX) and DSPE-PEG-anti-CD80, and the hUCMSCs were subjected to treatment for a further 48 hours. The supernatant was collected and centrifuged at 2000 × g for 30 minutes to eliminate cell remnants and particulate matter, subsequent to this, a rapid centrifugation process at 16,000 × g for 60 minutes, with all centrifugation procedures conducted at 4°C. The pelleted particles subsequently underwent a rinsing process using phosphate-buffered saline (PBS) to reconstitute the anti-CD80-MTX-EVs, which were either cryopreserved at −80°C or promptly utilized for ensuing experimental protocols. Detailed information regarding reagents were listed in the supporting information.

The morphology of the extracellular vesicles (EVs) was analyzed using transmission electron microscopy (TEM, model JEM-2100F, manufactured by Japan Electronics Co., Ltd.) to delineate their characteristics. The analysis of the size distribution profile of extracellular vesicles (EVs) was carried out via nanoparticle tracking analysis (NTA, ZetaView, Particle Metrix Inc., Germany). The encapsulation efficiency of methotrexate (MTX) within the EVs (MTX-EVs) was evaluated with high-performance liquid chromatography (HPLC). The concentration of MTX in the EVs was quantified by referencing a standard calibration curve.

Flow Cytometry

The EVs and anti-CD80-EVs were tagged with FITC-conjugated anti-Rat antibody by incubating for 15 minutes at 37°C. Post-incubation, the excess FITC-conjugated antibody was separated from the complexes by centrifugation. For the quantification of Tregs and Th1 cell populations in paw, gingival, and lymph node tissues, the cell suspensions were pelleted by centrifugation at 4°C, with the supernatant being discarded thereafter. The cells were subsequently labeled using FITC-conjugated anti-CD4 antibody, incubated for 30 minutes at 4°C. Another centrifugation at 4°C was performed to discard the supernatant, and the cells were then suspended in 200 μL of fixation/permeabilization reagent, followed by a 45-minute incubation at 4°C. After rinsing with 1× permeabilization buffer, the cells were incubated with PE-conjugated anti-T-bet and PE-conjugated anti-Foxp3 antibodies, following the manufacturer's protocol. This staining process took place in the dark for an additional 45 minutes at room temperature in flow cytometry staining buffer. Following two further washes, the cells were reconstituted in the same buffer as above prior to being analyzed by a flow cytometer (Beckman Coulter, USA). There were 10000 events collected during the analysis, and the SSC and FSC analysis strategy for each cell type were showed in Figure S7. Data processing and graphical illustration were carried out using FlowJo V10 software. Detailed information regarding reagents and antibodies were listed in the supporting information.

Western Blot

The protein concentrations of EVs, anti-CD80-EVs, and anti-CD80-MTX-EVs were quantified by employing a BCA reagent, the concentration of loading samples was 1 mg/mL. Subsequent to electrophoresis performed on the Bio-Rad system, the proteins, having been separated, were subsequently transferred onto a PVDF membrane from the gel. The membrane was then subjected to block using a 5% bovine serum albumin (BSA) solution at room temperature (RT) for a duration of 90 minutes. Following this, which was probed with primary antibodies specific to CD105, CD9, CD81, and β-actin, each diluted at a ratio of 1:1000, and incubated at 4°C overnight. After thorough washing with TBST buffer thrice, the membrane was exposed to the appropriate HRP-conjugated secondary antibody, diluted 1:10,000, and then it

was incubated for 1 hour at RT. In the case of CD80 antibody analysis, the membrane was directly treated with the HRP-conjugated secondary antibody under identical conditions, omitting the overnight incubation. The protein bands were ultimately revealed using a chemiluminescent detection kit (Millipore, USA) and captured using an imaging system (Tanon 4600, China). The uncropped pictures of the Western blotting bands are presented in Figure S8, and detailed information regarding reagents and antibodies were listed in the supporting information.

Isolation and Cultivation of Primary Macrophages

Macrophages derived from the bone marrow of C57BL/6 mice were isolated. Initially, the femur and tibia bones were dissected from the mice, and the bone marrow was flushed using a 21-gauge needle with ice-cold RPMI 1640 medium. The cells were then cultured in RPMI 1640 medium supplemented using 10% fetal bovine serum (FBS) and 50 ng/mL of macrophage colony-stimulating factor (M-CSF) for 7 days. And then, the medium was replaced. Following this differentiation period, the cells were ready for use in subsequent experiments. Detailed information regarding reagents were listed in the supporting information.

RNA-Sequencing

BMDMs were exposed to LPS (200 ng/mL) either alone or in combination with EVs or MTX-EVs (10 μg/mL) for 24 hours. The RNA was then isolated and underwent RNA-sequencing examination. The sequencing data was filtered with SOAPnuke by (1) Removing reads containing sequencing adapter; (2) Removing reads whose low-quality base ratio (base quality less than or equal to 15) is more than 20%; (3) Removing reads whose unknown base ('N' base) ratio is more than 5%, afterward clean reads were obtained and stored in FASTQ format. The subsequent analysis and data mining were performed on Dr. Tom Multi-omics Data mining system (https://biosys.bgi.com). Expression level of gene was calculated by RSEM (v1.3.1). The heatmap was drawn by pheatmap (v1.0.12) according to the gene expression difference in different samples. Essentially, differential expression analysis was performed using the DESeq2 (v1.34.0) (or DEGseq (v1.48.0) (or PoissonDis) with Q value ≤ 0.05 (or FDR ≤ 0.001). To take insight to the change of phenotype, KEGG (https://www.kegg.jp/) enrichment analysis of annotated different expression gene was performed by Phyper based on Hypergeometric test. The significant levels of terms and pathways were corrected by Q value with a rigorous threshold (Q value ≤ 0.05). Detailed information regarding reagents were listed in the supporting information.

RNA Extraction, Reverse Transcription, and qPCR

The RNA was isolated using TRIzol reagent (15–596-026, Invitrogen, USA) and subsequently reverse-transcribed into cDNA with reverse transcriptase. qRT-PCR was then performed using DNA amplification enzyme on a qRT-PCR system (Bio-Rad, USA). The qRT-PCR primer sequences are provided in detail within Table S1. The expression levels of each target gene were comparatively assessed utilizing the $2^{-\Delta\Delta Ct}$ approach to facilitate statistical evaluation. The expression levels of genes were adjusted by referencing the mean expression of all control samples, using GAPDH as the reference gene. All primers were designed using Primer Premier 5.0, primers specific detection was performed using NCBI Prime-BLAST tool. All PCR results were validated through three independent experimental replicates. Detailed information regarding reagents were listed in the supporting information.

Animal Experiment

Female DBA/1J mice, aged 6 weeks, designated for the rheumatoid arthritis (RA) model, were procured from Keaoke Biotechnology Co., Ltd (Xi'an, China). Similarly, 6-week-old female C57BL/6 mice, intended for the PD model, were sourced from the Animal Center of the Air Force Medical University (Xi'an, China). All experimental protocols underwent review and were sanctioned by the Animal Protection Committee at the Air Force Medical University (Xi'an, China). The female DBA/1J mice with 6-week-old were utilized for the RA model, while the C57BL/6 mice with same week age were employed for the PD model. For each animal model, the mice were allocated into four separate groups, each consisting of eight individuals. One group served as the control for either RA or PD, and the remaining three groups were designated for treatment with EVs, anti-CD80-EVs, and anti-CD80-MTX-EVs, respectively. The CIA (collagen-induced arthritis) animal model was established following a previously described protocol. In brief, DBA/1J

mice received an intradermal injection at the tail's base, consisting of 200 μg of bovine type II collagen mixed in 100 μL of CFA. On day 21, a booster immunization was performed using IFA. Post-immunization, PBS and EVs (40 μg/50 μL) were administered via tail vein injection and intraperitoneal injection, respectively, every 5 days for a total duration of 30 days. The hind limb arthritis severity in CIA mice was categorized into four grades: 0, 1, 2, 3, with 4 signifying the highest severity. The cumulative score for each paw was calculated, allowing for a potential maximum score of 16 per mouse. Detailed information regarding reagents were listed in the supporting information.

The experimental periodontitis model was induced using a ligature-based method. Specifically, the mice were anesthetized, and their mouths were held open via a spreader. A segment of 15–20 cm from a 5–0 sterile silk suture ligature was utilized, featuring two central knots spaced approximately 2 mm apart, was prepared. The ligature was then securely placed between the first and second molars (M1 and M2), and any excess thread was trimmed away. After 14 days, 10 μL of saline or EVs, anti-CD80-EVs, and anti-CD80-MTX-EVs (20 μg) was administered into the right maxillary palatal gingiva between the first and second upper molars. This treatment was repeated every 2 days for a duration of 2 weeks in each group.

Cytokine Measurement

The levels of IL-10, IFN-γ, TNF-α and TGF-β in both the serum and gingival tissue collected from CIA and ligature-induced PD mice were quantified using ELISA kit, adhering to the manufacturer's protocol. Absorbance was measured at 450 nm using microplate reader (Bio-Rad, USA). Detailed information regarding reagents were listed in the supporting information.

Micro-CT Analysis

To assess the extent of periodontal recession, the maxillary jaws were subjected to scanning and subsequent analysis using the Quantum GX micro-CT system (PerkinElmer, USA). Following the scanning process, the images obtained were reconstructed using Mimics software (Materialise, Belgium). The height of the alveolar bone was quantified by measuring the distance from the cementoenamel junction (CEJ) to the crest of the alveolar bone at four distinct sites across two molars.

In vivo Tracing of EVs, Anti-CD80-EVs and Anti-CD80-MTX-EVs

EVs, anti-CD80-EVs, and anti-CD80-MTX-EVs were initially labeled with DiR. Subsequently, these labeled EVs were administered to CIA mice and ligature-induced PD mice via intravenous injection or local periodontal injection, with each mouse receiving a volume of 10 μL. At predetermined intervals, the CIA and ligature-induced PD mice were humanely euthanized. Following this, the hearts, livers, spleens, lungs, kidneys, paws, periodontal tissues, and lymph nodes were carefully excised and harvested. The biodistribution of the labeled EVs, anti-CD80-EVs, and anti-CD80-MTX-EVs within these organs was assessed through fluorescence imaging, utilizing a Maestro automated in vivo imaging system (Caliper, USA). Detailed information regarding reagents were listed in the supporting information.

Histological Analysis

Following a therapeutic observation period of 30 days for CIA mice and 14 days for ligature-induced PD mice, the ankle joints from the CIA group and the maxillary jaws from the PD group were preserved in a 4% polyformaldehyde solution for a duration of 48 hours. Following this, the specimens underwent a decalcification process in a 17% EDTA solution (pH adjusted to 7.4) over a span of 21 days, after which they were encased in paraffin. Thin sections of the periodontal tissue, precisely 5 micrometers in thickness, were prepared for H&E staining. Similarly, 5-micrometer sections of the ankle joints were treated with Saffron solid green and H&E and staining, meticulously following the protocols outlined by the producer. Detailed information regarding reagents were listed in the supporting information.

Statistical Analysis

All experimental data are expressed as mean ± SD. Statistical analyses were conducted using GraphPad Prism 9.0 with statistical significance defined as $P < 0.05$. Prior to the analysis, dataset normality was verified through Shapiro–Wilk

testing ($\alpha = 0.05$) and variance homogeneity assessed via Levene's test. For datasets satisfying these criteria, parametric analyses were performed using: (1) unpaired two-tailed Student's t-tests for pairwise comparisons; (2) one-way ANOVA with Tukey's multiple comparisons test for multi-group analyses. Non-parametric datasets were evaluated with Mann–Whitney *U*-tests (pairwise) or Kruskal–Wallis tests (multi-group) followed by Dunn's post-hoc correction. All experimental observations were retained for analysis without exclusion.

Results

The Population of $CD80^+$ Macrophages Was Elevated in CIA and PD Mice

Macrophages have a key immunomodulatory effect in the progression and resolution of chronic inflammatory diseases, such as RA and PD.[26–28] To achieve targeted regulation of macrophages in the inflammation, we first detected the expression of CD80 and CD86 (representative biomarkers of pro-inflammatory polarized macrophages) in macrophages in CIA and PD mice by flow cytometry. The results revealed a considerable rise in the proportion of macrophages in the swollen joints of CIA mice, with $CD80^+$ macrophages showing the most significant increase followed by $CD86^+$ macrophages ($P < 0.001$) (Figure 1A and D). Similarly, increased proportion of $CD80^+$ macrophages were detected in the popliteal lymph nodes compared to the control group ($P < 0.001$) (Figure 1B and E), but they showed no significance in spleen compared to the control group (Figure 1C and F). As expected, significant accumulation of $CD80^+$ macrophages were also detected in the gingival tissue, cLN of experimental periodontitis induced by silk ligature, as indicated by the higher proportion ($P < 0.01$and $P < 0.001$) (Figure 1G, J, H and K). The percentage of $CD80^+$ macrophages in the spleen exhibited no substantial variation when contrasted with the control group (Figure 1I and L). The findings suggested that $CD80^+$ macrophages are elevated in both the affected tissue and the lymphatic nodes that drain the area in chronic inflammatory conditions, potentially representing a therapeutic target for the management of inflammatory disorders.

Construction and Characterization of Anti-CD80-MTX-EVs

Based on the discovery of $CD80^+$ macrophage aggregation in CIA and PD mice, we designed engineered EVs (anti-CD80-MTX-EVs) to target $CD80^+$ macrophages followed with intracellular MTX delivery to precisely regulate the immune function. To prepare these engineered EVs, we first conjugated the phospholipid (DSPE-PEG-NH_2) with CD80 antibody through amidation reaction. The as-synthesized DSPE-PEG-anti-CD80 was then incubated with hUCMSCs for 24 hours. During this time, the DSPE section of these molecules would rapidly insert the phospholipid layer of hUCMSCs to generate anti-CD80 grafted cells, resulting in the further production of the anti-CD80-EVs. The cell supernatant was then centrifuged at differential speed and anti-CD80-EVs were ultimately enriched in the form of precipitates. HUCMSCs were also supplemented with MTX to obtain MTX loaded EVs (MTX-EVs). More importantly, we added both DSPE-PEG-anti-CD80 and MTX to hUCMSCs to obtain anti-CD80-MTX-EVs (Figure 2A). The level of MTX encapsulated within MTX-EVs was roughly 0.4 μg/mL, as analyzed via HPLC (Figure 2B).

As depicted in Figure 2C, the characteristic peaks of P=O from DSPE at 1350 cm^{-1} and C-H from PEG at about 2800 cm^{-1} were detected in Fourier transform infrared (FTIR) spectrum of DSPE-PEG-anti-CD80 provided direct evidence for the successful combination of DSPE-PEG-NH_2 with anti-CD80. Moreover, the additional P signals observed in the DSPE-PEG-anti-CD80 compared with the pure CD80 antibody also indicated the formation of DSPE-PEG-anti-CD80 as design (Figure 2D). Since the anti-CD80 antibody is an IgG derived from rats, we detected rat IgG in anti-CD80-EVs by ELISA. The quantitative detection of the concentration of rat IgG indicated that anti-CD80-EVs were bound to a large amount of rat IgG, while rat IgG was almost undetectable in EVs ($P < 0.001$), indicating the successful construction of anti-CD80 EVs (Figure 2E). After co-incubation with an anti-rat IgG second antibody conjugated with FITC, stronger FITC fluorescence was also detected in anti-CD80 EVs compared with the EVs group by flow cytometry ($P < 0.0001$) (Figure 2F and G) and immunofluorescence ($P < 0.05$) (Figure S1A), further confirming the successful formation of anti-CD80-EVs. To examine the cellular internalization of EVs and anti-CD80-EVs by macrophages, we treated macrophages with PKH67-labeled EVs and anti-CD80-EVs. The anti-CD80-EVs group exhibited a notably

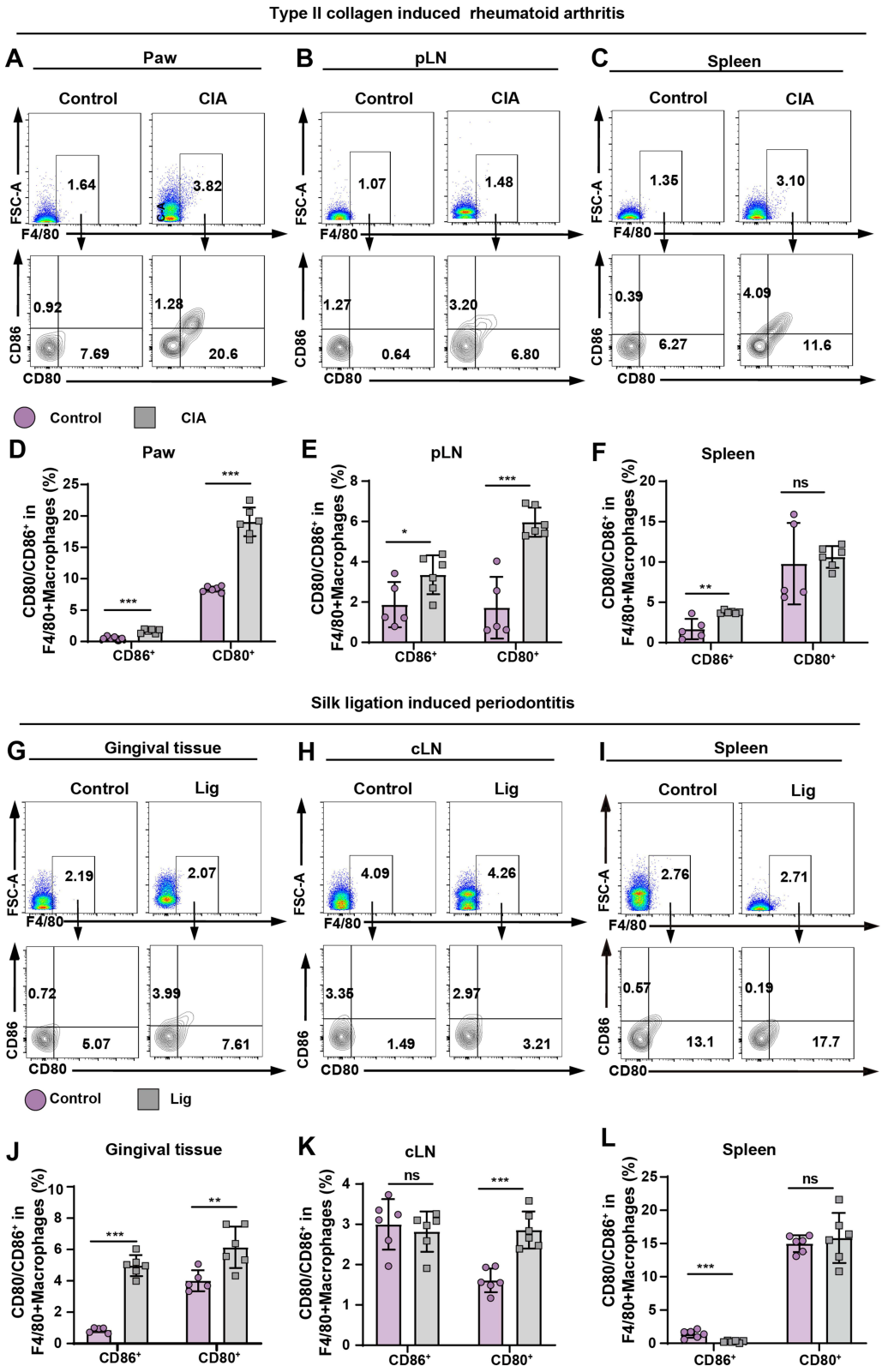

Figure 1 CD80$^+$ macrophages were increased in CIA and PD mice. (**A-C**) Frequency of CD80$^+$/CD86$^+$ macrophages in paw (**A**), pLN (**B**) and spleen (**C**) in representative flow plots of control and CIA mice. (**D-F**) Histograms of CD80$^+$/CD86$^+$ macrophages populations in paw (**D**), pLN (**E**) and spleen (**F**) of control and CIA mice. (**G-I**) Frequency of CD80$^+$/CD86$^+$ macrophages in gingival tissue (**G**), cLN (**H**) and spleen (**I**) of control and ligature-induced PD mice. (**J-L**) Histograms of CD80$^+$/CD86$^+$ macrophages populations in gingival tissue (**J**), cLN (**K**) and spleen (**L**) of control and ligature-induced PD mice. (n ≥ 5, *P < 0.05, **P < 0.01, ***P < 0.001).
Abbreviation: ns, not significant.

https://doi.org/10.2147/IJN.S517357

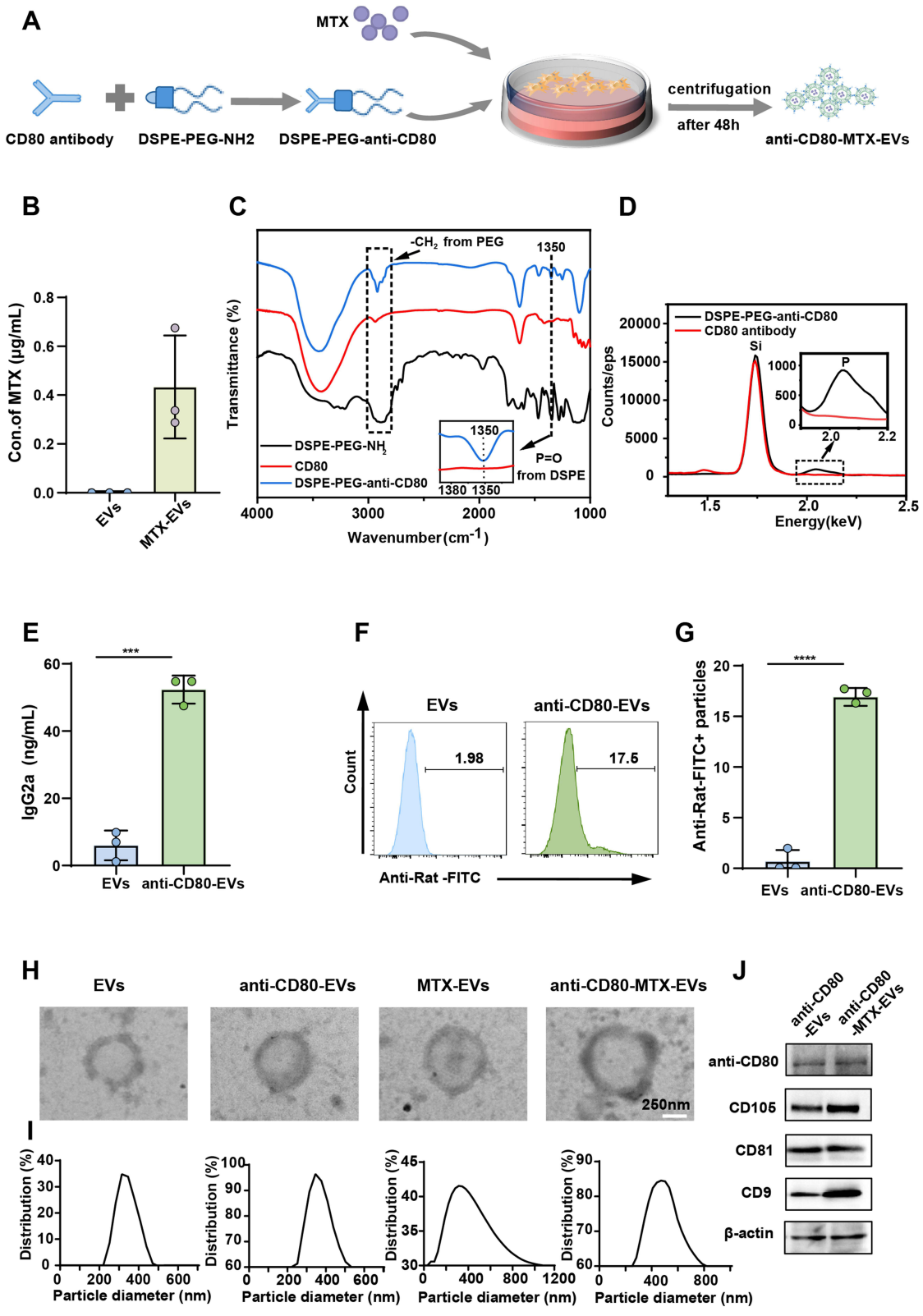

Figure 2 Construction and characterization of anti-CD80-MTX-EVs. (**A**) Schematic representation of the construction of anti-CD80-MTX-EVs. (**B**) The concentration of MTX loaded in MTX-EVs was detected by HPLC. (**C**) Fourier transform infrared spectrometer (FTIR) of DSPE-PEG-NH2, CD80 antibody and DSPE-PEG-anti-CD80. (**D**) Energy-dispersive x-ray spectra (EDS) of DSPE-PEG-anti-CD80 and CD80 antibody. (**E**) The concentration of IgG2a in EVs and anti-CD80-EVs. (**F**) anti-Rat-FITC staining of EVs and anti-CD80-EVs in representative flow plots. (**G**) Histogram of anti-Rat-FITC staining of EVs and anti-CD80-EVs. (**H–I**) Representative TEM image (**H**) and size distribution (**I**) of EVs, anti-CD80-EVs, MTX-EVs and anti-CD80-MTX-EVs. Scale bars, 250 nm. (**J**) The protein expression of CD80, CD105, CD81 and CD9 for anti-CD80-EVs and anti-CD80-MTX-EVs. (n = 3, ***P < 0.001, ****P < 0.0001).

Abbreviation: ns, not significant.

higher green fluorescence signal compared to the EVs group ($P < 0.01$) (Figure S1B), indicating the preferential uptake of anti-CD80-EVs by macrophages (Supplementary materials and methods).

The TEM and DLS were used to observe the morphology and size of different EVs, respectively. TEM images showed typical double-layer circular structures of EVs, anti-CD80-EVs, MTX-EVs and anti-CD80-MTX-EVs (Figure 2H). The NTA results indicated that the dimensions of anti-CD80-EVs was the same as EVs (approximately 350nm), the diameter of MTX-EVs was approximately 400nm, while the diameter of anti-CD80-MTX-EVs slightly increased (approximately 450nm) (Figure 2I). Moreover, the anti-CD80-EVs and anti-CD80-MTX-EVs showed high expression of CD80 antibody, indicating that the CD80 antibody was successfully combined to the vesicles, as well as mesenchymal stem cell marker CD105 were expressed in EVs, MTX-EVs (Figure S2), anti-CD80-EVs and anti-CD80-MTX-EVs (Figure 2J). Moreover, the vesicle-associated protein markers CD81 and CD9 were detected in EVs, MTX-EVs (S2), anti-CD80-EVs, and anti-CD80-MTX-EVs (Figure 2J), suggesting that the production of engineered EVs did not drastically alter their intrinsic physical characteristics.

Anti-CD80-MTX-EVs Promote Anti-Inflammatory Transformation of Macrophages to Induce Tregs Production

We hypothesized that anti-CD80-MTX-EVs would target $CD80^+$ macrophages, reshape macrophages function towards an anti-inflammatory profile, and thereby suppress the excessive activation of T cells. To test this hypothesis, we first wanted to see whether MTX-EVs could promote anti-inflammatory transformation of macrophages. RNA sequencing was carried out to detect changes of related genes in BMDMs after LPS, EVs and MTX-EVs treatment. As indicated by heat map and KEGG pathway, TGF-β pathway-related genes were enriched in the LPS + MTX-EVs treated BMDMS group (Figure 3A and B). Specifically, the gene expression of Tgfb2, Tgfb3, Bmbpr2 and Smad5 in BMDMs with treatment of LPS + MTX-EVs were significantly increased compared with other groups ($P < 0.01$) (Figure 3C–F). BMDMs with the treatment of LPS + MTX-EVs also showed increased TGF-β expression compared with other groups by ELISA analysis ($P < 0.01$) (Figure 3G).

Further, we examined the ability of anti-CD80-MTX-EVs to target $CD80^+$ macrophages and induce Treg cells production. The proportion of $CD80^+$ BMDMs after LPS treatment was significantly elevated by flow cytometry. Moreover, the proportion of $CD80^+$ BMDMs was reduced by the treatment of EVs, anti-CD80-EVs and anti-CD80-MTX-EVs to varying degrees. Anti-CD80-MTX-EVs exhibited significantly more effective inhibition of the proportion of $CD80^+$ BMDMs with LPS treatment than EVs and anti-CD80-EVs ($P < 0.001$) (Figure 3H). Then, we co-cultured BMDMs of these groups with T cells from cLN of PD mice. Treg cells induced by macrophages after treatment by engineered EVs were evaluated (Figure 3I). As anticipated, the percentage of $CD4^+$ $Foxp3^+$ T cells in anti-CD80-EVs and anti-CD80-MTX-EVs groups were increased, with anti-CD80-MTX-EVs showing a more significant induction effect on Treg cells ($P < 0.01$) (Figure 3J and K). These results strongly demonstrate that anti-CD80-MTX-EVs effectively target $CD80^+$ macrophages and promote TGF-β production, which induces Treg cells amplification in vitro.

Anti-CD80-MTX-EVs Effectively Alleviate CIA and Suppress Inflammation

To assess the therapeutic efficacy of anti-CD80-MTX-EVs on chronic inflammation in vivo, 40 μg EVs, anti-CD80 EVs, and anti-CD80 MTX-EVs were, respectively, injected into CIA mice via tail vein every 5 days after immunization (Figure 4A). As expected, EVs, anti-CD80 EVs and anti-CD80 MTX-EVs effectively reduced DAI scores and incidence rate of arthritis, and inhibited joint swelling, which was manifested as smaller paw thickness and ankle diameter. Meanwhile, anti-CD80 MTX-EVs showed the most significant treatment effect on CIA mice ($P < 0.05$) (Figure 4B and C). Histological analysis of joint tissue revealed that anti-CD80-MTX-EVs treatment prevented joint injury and infiltration of inflammatory cells into joint tissue as measured by a histological activity index (Figure 4D and E). In addition, anti-CD80-MTX-EVs also reduced the levels of TNF-α and IFN γ in serum most significantly ($P < 0.01$) (Figure 4F and G). The concentration of IL-10 and TGF-β in the anti-CD80-MTX-EVs treated mice also showed an increase compared with other EVs groups ($P < 0.05$) (Figure 4I and H). To know the biodistribution of EVs in CIA mice after injection, we used the in vivo imaging system and found that fluorescently labeled EVs in different group

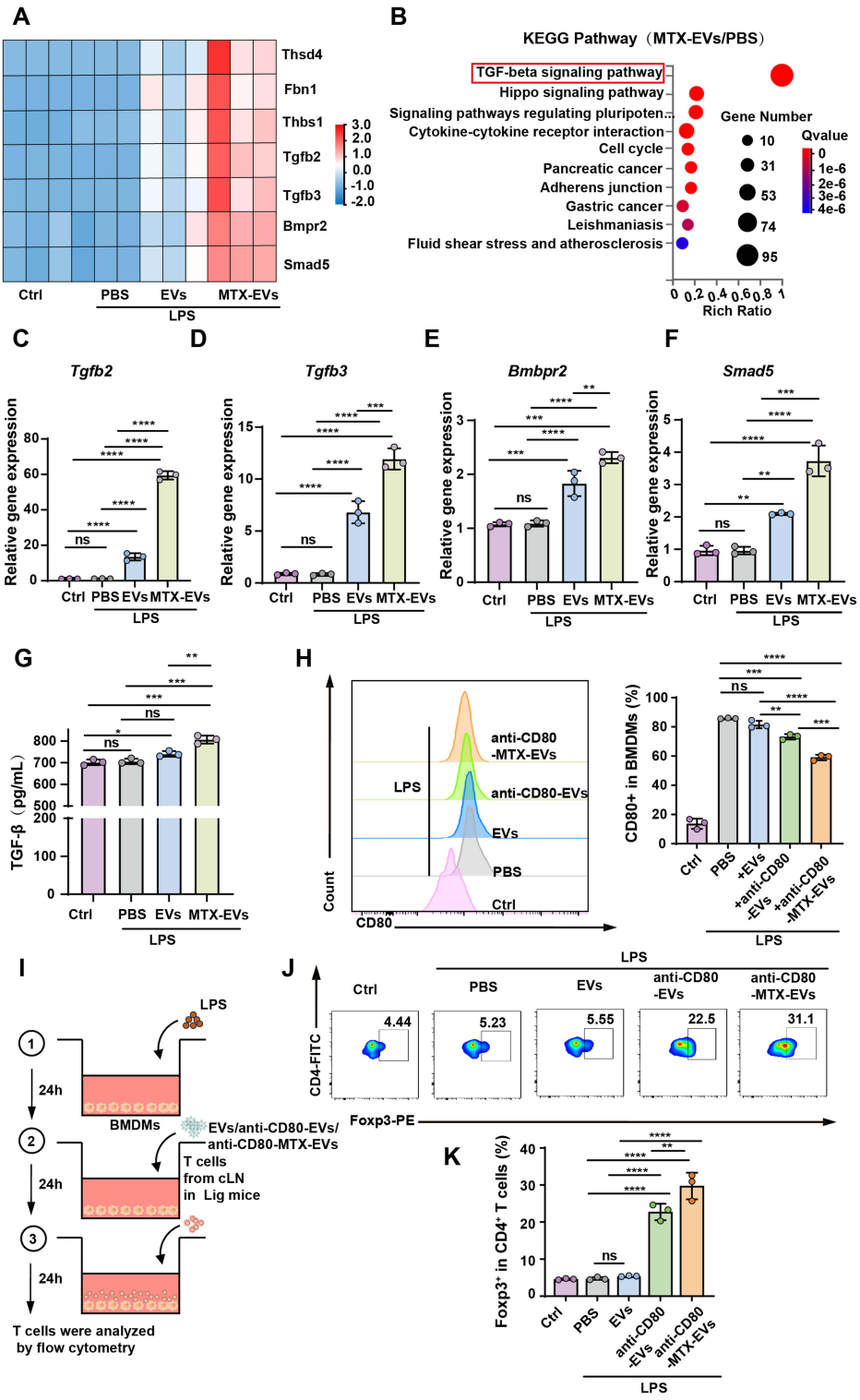

Figure 3 Anti-CD80-MTX-EVs promote anti-inflammatory transformation of macrophages to induce Tregs production. (**A**) Heatmap depicts differential TGF-β related genes expression in BMDMs, LPS + BMDMs, LPS + BMDMs + EVs and LPS + BMDMs + MTX-EVs. (**B**) The correlated KEGG pathways were predicted in macrophages. (**C-F**) Representative qRT-PCR results for TGF-β related genes Tgfb2 (**C**), Tgfb3 (**D**), Bmbpr2 (**E**), and Smad5 (**F**). (**G**) The expression of TGF-β in BMDMs (Ctrl), LPS + BMDMs, LPS + BMDMs + EVs and LPS + BMDMs + MTX-EVs was detected by ELISA. (**H**) Representative flow plot and summary histogram (right) of the CD80 proportion in BMDMs (Ctrl), LPS + BMDMs, LPS + BMDMs + EVs, LPS + BMDMs + anti-CD80-EVs and LPS + BMDMs + anti-CD80-MTX-EVs. (**I**) Schematic diagram of BMDMS and T cell co-culture process. (**J**) Representative flow plots of $CD4^+$ $Foxp3^+$ cells populations in BMDMS, LPS + BMDMs, LPS + BMDMs + EVs, LPS+BMDMs + anti-CD80-EVs and LPS + BMDMs + anti-CD80-MTX-EVs. (**K**) Histogram of $CD4^+$ $Foxp3^+$ T cells in BMDMs, LPS + BMDMs, LPS + BMDMs + EVs, LPS + BMDMs + anti-CD80-EVs and LPS + BMDMs + anti-CD80-MTX-EVs. (n = 3). (*P < 0.05, **P < 0.01, ***P < 0.001, ****P < 0.0001).

Abbreviation: ns, not significant.

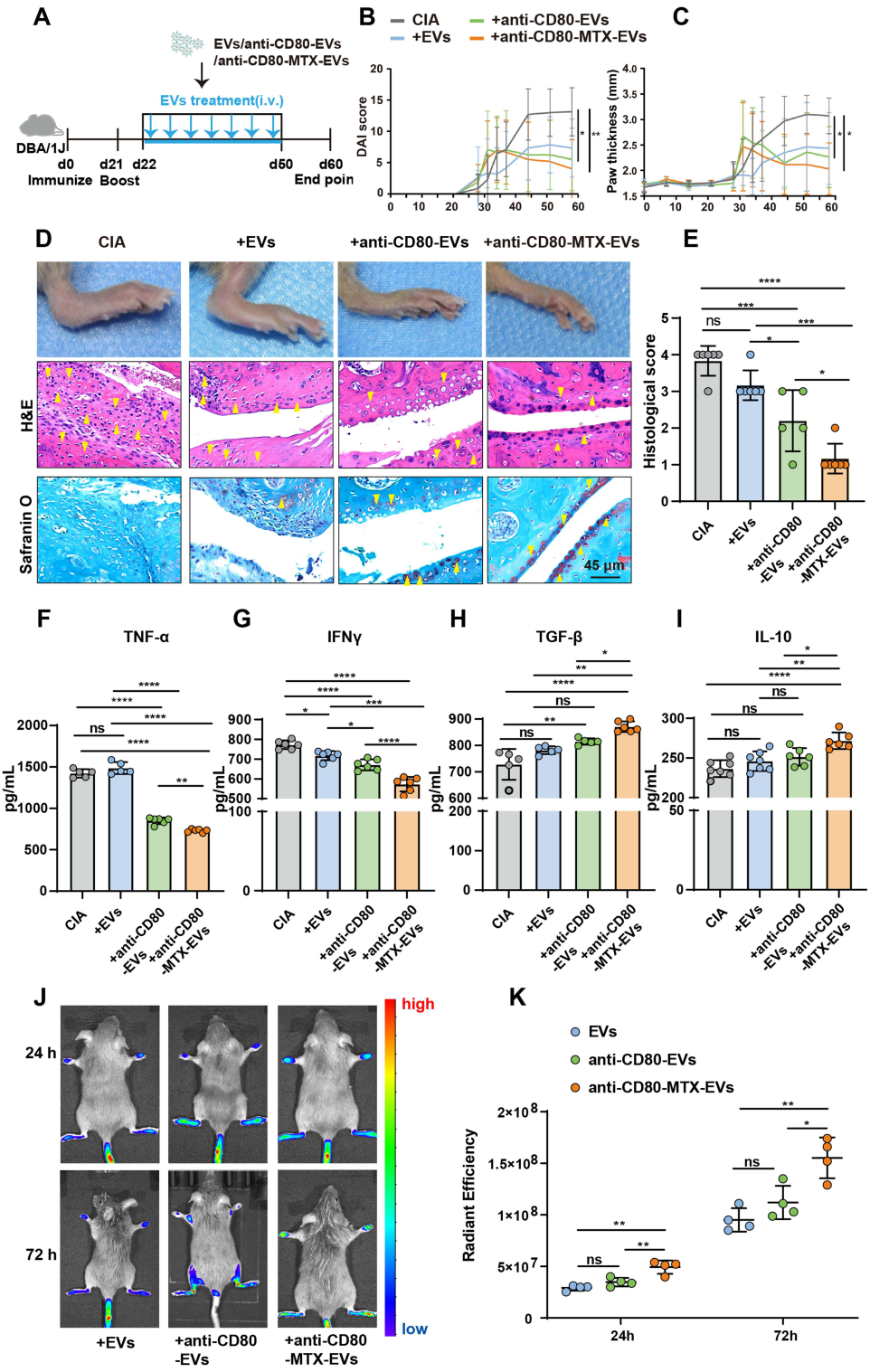

Figure 4 Anti-CD80-MTX-EVs effectively alleviate CIA and inhibit inflammation. (**A**) Schematic diagram of experimental design for treating CIA mice with EVs, anti-CD80-EVs and anti-CD80-MTX-EVs. (**B**) Mean clinical score measurements and (**C**) paw thickness of CIA mice and CIA mice treated with EVs, anti-CD80-EVs and anti-CD80-MTX-EVs. (**D**) Representative conventional camera, H&E and Safranin solid green staining images of hind paws of CIA mice and CIA mice treated with EVs, anti-CD80-EVs and anti-CD80-MTX-EVs. Scale bars, 45 μm. (**E**) Histological score analysis of the ankle joints of CIA mice and CIA mice treated with EVs, anti-CD80-EVs and anti-CD80-MTX-EVs (n ≥ 5). (**F-I**) The expression of the pro-inflammatory/anti-inflammatory cytokine TNF-α (**F**), IFN γ (**G**), TGF-β (**H**) and IL-10 (**I**) in serum of the CIA mice and CIA mice treated with EVs, anti-CD80-EVs and anti-CD80-MTX-EVs (n = 6). (**J**) In vivo distribution of EVs, anti-CD80-EVs and anti-CD80-MTX-EVs in CIA mice. (**K**) Quantitative analysis of the fluorescence intensity of the paw in CIA mice treated with EVs, anti-CD80-EVs and anti-CD80-MTX-EVs (n = 4). (*P < 0.05, **P < 0.01, ***P < 0.001, ****P < 0.0001).
Abbreviation: ns, not significant.

https://doi.org/10.2147/IJN.S517357

aggregated in inflamed joint at 24 and 72 hours after intravenous injection. Anti-CD80-MTX-EVs showed higher fluorescence intensity compared to the EVs group and anti-CD80-EVs group (Figure 4J, K and Figure S3A, B), indicating that anti-CD80-MTX-EVs can effectively target $CD80^+$ macrophages in the inflammatory joints in vivo ($P < 0.05$).

Furthermore, immune cell phenotype in inflamed joint showed that anti-CD80-MTX-EVs treatment resulted in the most significant reduction of $F4/80^+$ $CD80^+$ cells compared to other CIA groups, as well as in pLN ($P < 0.001$) (Figure 5A–C). Strikingly, further studies found that, as demonstrated by the higher $CD4^+$ $Foxp3^+$ T cells proportion, anti-CD80-MTX-EVs was the most effective in inducing Treg cells compared to other groups ($P < 0.05$) (Figure 5D–F), while also significantly promoting the secretion of IL-10 in $CD4^+$ T cells ($P < 0.001$) (Figure 5G–I). In addition, anti-CD80-EVs and anti-CD80-MTX-EVs also reduced the proportion of $CD4^+$ T-bet^+ T cells and IFN γ secretion by $CD4^+$ T cells in the paw and pLN ($P < 0.05$) (Figure 5J-L and Figure S4A-C), indicating a relief of the inflammation. These data collectively indicate that anti-CD80-MTX-EVs reduce inflammation and restore tissue homeostasis to alleviate CIA.

Anti-CD80-MTX-EVs Alleviate Experimental Periodontitis and Prevent Bone Loss

In PD, the gingiva exhibits heightened inflammatory reactions, resulting in immunopathological changes and the erosion of structural bone.[29] We explored the anti-inflammatory function of anti-CD80-MTX-EVs in ligature-induced PD mice. EVs, anti-CD80-EVs and anti-CD80-MTX-EVs (40 μg in 10 μL PBS) were, respectively, injected at the same sites between the first and second molars in ligature-induced PD mice. The mice with induced ligatures received PBS injections as the control group. Subsequent Micro-CT analysis and H&E staining were conducted to measure the alveolar bone loss in the periodontal tissues following a 14-day treatment with EVs, anti-CD80-EVs, and anti-CD80-MTX-EVs (Figure 6A). The Lig group experienced significant loss of alveolar bone, a condition that was not evident in the ligature-induced periodontitis (PD) mice following treatment with anti-CD80-EVs and anti-CD80-MTX-EVs, as indicated by the measurement from the cementoenamel junction (CEJ) (Figure 6B–G). Anti-CD80-MTX-EVs treatment significantly reduced the concentration of TNF-α and IFN γ in the gingival tissue compared to other ligature groups ($P < 0.05$) (Figure 6H and I) and effectively increased the concentration of TGF-β and IL-10 in ligature-induced PD mice ($P < 0.001$) (Figure 6J and K). In addition, we also observed the biodistribution of anti-CD80-MTX-EVs in ligature-induced PD mice treated with EVs, anti-CD80-EVs and anti-CD80-MTX-EVs. The findings indicated that following local administration into the mouse periodontium, the fluorescence-tagged anti-CD80-MTX-EVs demonstrated significantly greater accumulation in the periodontal tissue at both 24 and 72 hour intervals, as opposed to the remaining groups ($P < 0.05$) (Figure 6L, M and Figure S5A, B).

Then, we also evaluated the changes of immune cells in the gingival tissue and cLN of ligature-induced PD mice and ligature-induced PD mice with EVs, anti-CD80-EVs and anti-CD80-MTX-EVs treatment. The flow cytometry results showed that anti-CD80 EVs and anti-CD80 MTX-EVs treatments significantly reduced the proportion of $CD80^+$ macrophages in gingival tissue ($P < 0.0001$) (Figure 7A and B). EVs, anti-CD80 EVs, and anti-CD80 MTX-EVs treatments significantly reduced the proportion of $CD80^+$ macrophages in cLN. Among them, anti-CD80-MTX-EVs showed the most significant effect in blocking CD80 expression of macrophages ($P < 0.05$) (Figure 7A and C). Flow cytometry analysis of T cells also showed that anti-CD80-MTX-EVs treatment can effectively promote $CD4^+$ $Foxp3^+$ T cell differentiation ($P < 0.0001$) (Figure 7D–F) and activate IL-10 secretion by $CD4^+$ T cells ($P < 0.01$) (Figure 7G–I). Moreover, anti-CD80-MTX-EVs treatment had the most prominent function of reducing $CD4^+$ T-bet^+ T cells and IFN γ secretion by $CD4^+$ T cells in ligature-induced PD mice ($P < 0.01$) (Figure 7J-L and Figure S6A-C). In summary, these results provide convincing evidence that anti-CD80-MTX-EVs delay the progression of periodontitis and prevent bone loss.

Discussion

In this study, we successfully engineered vesicles capable of specifically targeting inflammatory macrophages for MTX delivery, thereby regulating the inflammatory response of macrophages, particularly in inducing Treg cells and promoting immune tolerance. Anti-CD80-MTX-EVs effectively suppressed CD80 expression in macrophages, enhanced TGF-β secretion by macrophages, and facilitated the generation of Treg cells. Furthermore, anti-CD80-MTX-EVs reduced the population of $CD80^+$ macrophages while promoting Treg cell generation and inhibiting Th1 cell differentiation

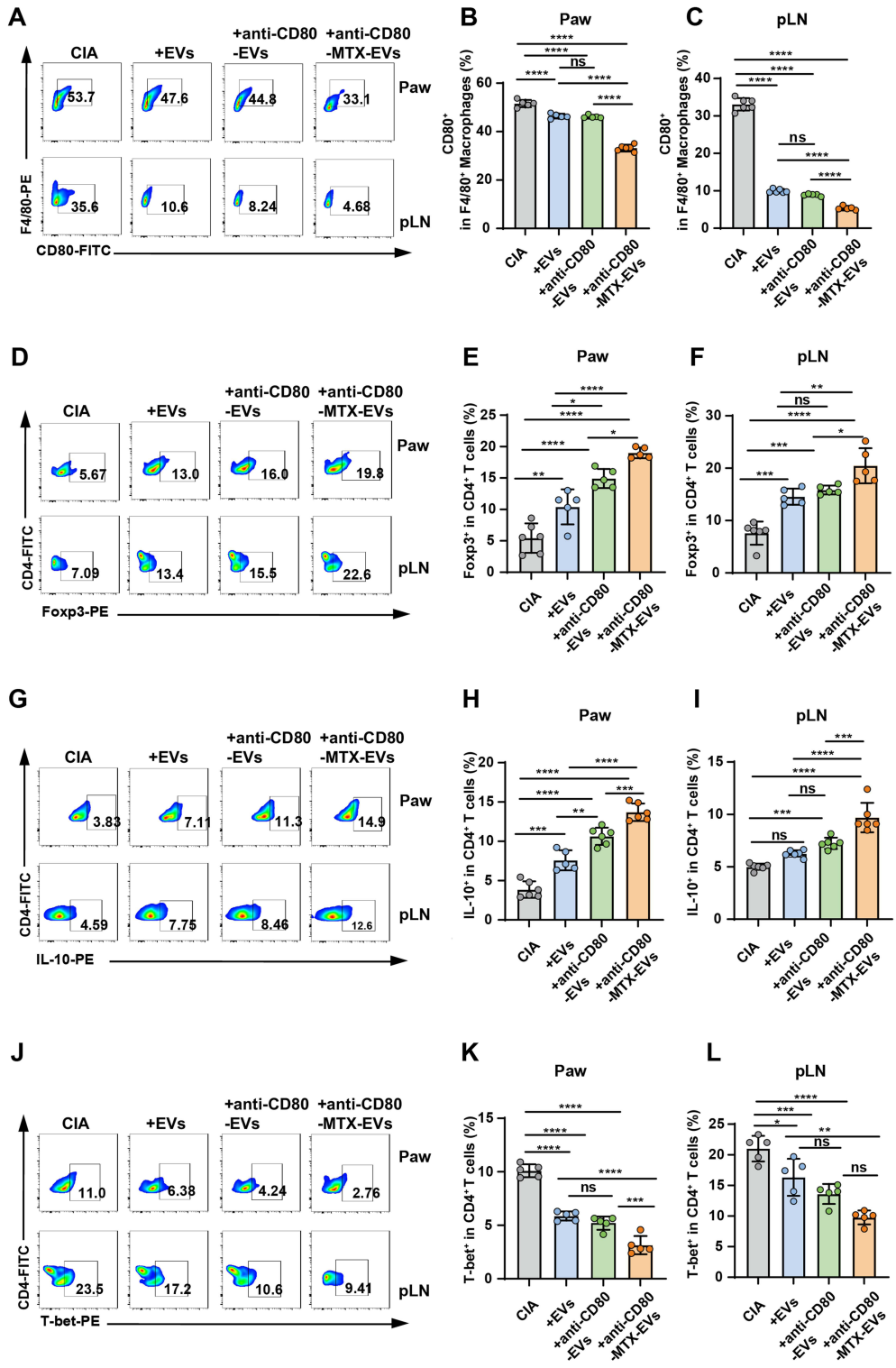

Figure 5 Anti-CD80-MTX-EVs induce immune tolerance and restore tissue homeostasis in CIA mice. (**A**) Representative flow plots and of $CD80^+$ macrophages populations in CIA mice and CIA mice treated with EVs, anti-CD80-EVs and anti-CD80-MTX-EVs. (**B**–**C**) Histogram of $CD80^+$ macrophages populations in paw (**B**) and pLN tissue (**C**) in CIA mice and CIA mice treated with EVs, anti-CD80-EVs and anti-CD80-MTX-EVs. (**D**) Representative flow plots of $CD4^+$ $Foxp3^+$ cells populations in CIA mice and CIA mice treated with EVs, anti-CD80-EVs and anti-CD80-MTX-EVs. (**E-F**) Histogram of $CD4^+$ $Foxp3^+$ cells populations in paw (**E**) and pLN tissue (**F**) in CIA mice and CIA mice treated with EVs, anti-CD80-EVs and anti-CD80-MTX-EVs. (**G**) Representative flow plots of $CD4^+$ IL-10^+ cells populations in CIA mice and CIA mice treated with EVs, anti-CD80-EVs and anti-CD80-MTX-EVs. (**H-I**) Histogram of $CD4^+$ IL-10^+ cells populations in paw (**H**) and pLN tissue (**I**) in CIA mice and CIA mice treated with EVs, anti-CD80-EVs and anti-CD80-MTX-EVs. (**J**) Representative flow plots of $CD4^+$ T-bet^+ cells populations in CIA mice and CIA mice treated with EVs, anti-CD80-EVs and anti-CD80-MTX-EVs. (**K-L**) Histogram of $CD4^+$ T-bet^+ cells populations in paw (**K**) and pLN tissue (**L**) in CIA mice and CIA mice treated with EVs, anti-CD80-EVs and anti-CD80-MTX-EVs. (n ≥ 5, ns, not significant, *P < 0.05, **P < 0.01, ***P < 0.001, ****P < 0.0001).

https://doi.org/10.2147/IJN.S517357

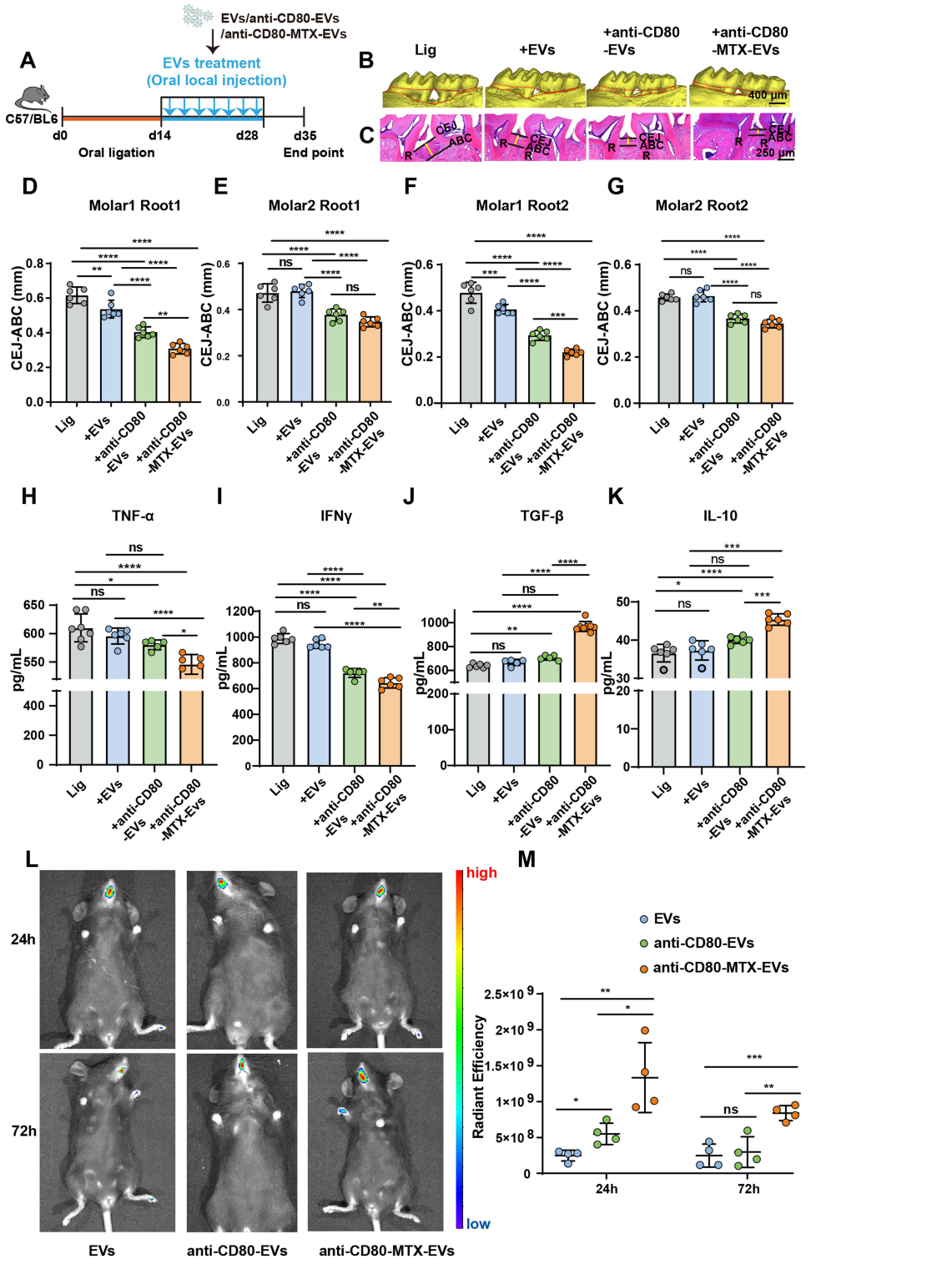

Figure 6 Anti-CD80-MTX-EVs alleviate experimental periodontitis and prevent bone loss. (**A**) Schematic diagram of experimental design for treating ligature-induced PD mice with EVs, anti-CD80-EVs and anti-CD80-MTX-EVs (**B-C**) The alveolar bone loss of ligature-induced PD mice and ligature-induced PD mice treated with EVs, anti-CD80-EVs and anti-CD80-MTX-EVs was determined by micro-CT (**B**) and H&E staining (**C**). Scale bar, 400 μm, 250 μm. (**D-G**) Four sites for two molars (one site for each root of one tooth) Molar1 Root1 (**D**), Molar2 Root1 (**E**), Molar1 Root2 (**F**) and Molar2 Root2 (**G**) of ligature-induced PD mice and ligature-induced PD mice treated with EVs, anti-CD80-EVs and anti-CD80-MTX-EVs were analyzed morphometrically. (**H-K**) The expression of the gingival tissue inflammatory/anti-inflammatory cytokine TNF-α (**H**), IFN γ (**I**), TGF-β (**J**) and IL-10 (**K**) of the ligature-induced PD mice and ligature-induced PD mice treated with EVs, anti-CD80-EVs and anti-CD80-MTX-EVs. (**L**) In vivo distribution of EVs, anti-CD80-EVs and anti-CD80-MTX-EVs in ligature-induced PD mice. (**M**) Quantitative analysis of the fluorescence intensity of the gingival tissue in ligature-induced PD mice and ligature-induced PD mice treated with EVs, anti-CD80-EVs and anti-CD80-MTX-EVs. (n ≥ 5, ns, not significant, *P < 0.05, **P < 0.01, ***P < 0.001, ****P < 0.0001).
Abbreviations: CEJ, Cementoenamel junction; ABC, Alveolar bone crest.

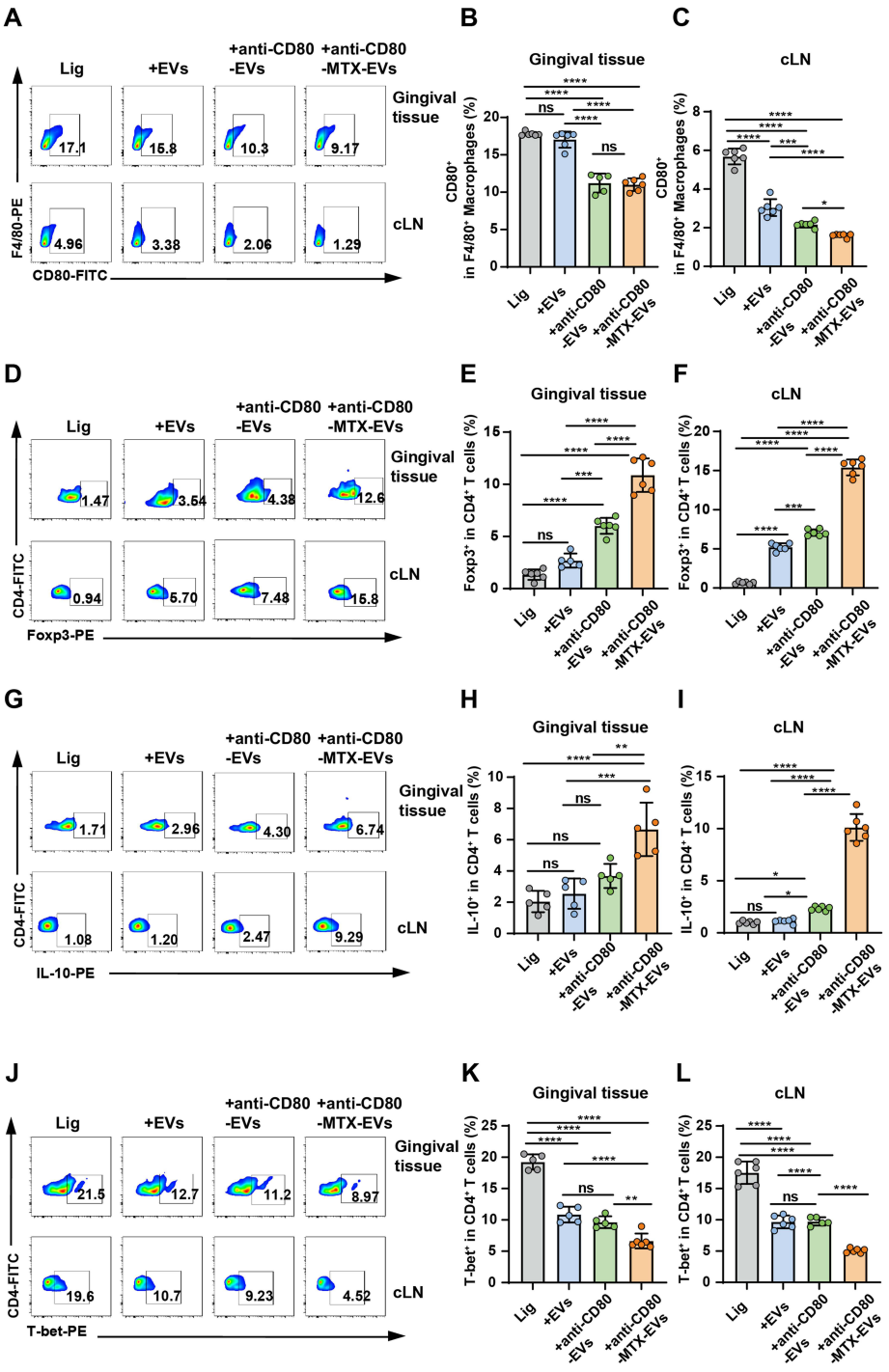

Figure 7 Anti-CD80-MTX-EVs inhibit inflammation and restore tissue homeostasis in ligature-induced PD mice. (**A**) Representative flow plots of $CD80^+$ macrophages populations in ligature-induced PD mice and ligature-induced PD mice treated with EVs, anti-CD80-EVs and anti-CD80-MTX-EVs. (**B-C**) Histogram of $CD80^+$ macrophages populations in gingival tissue (**B**) and cLN (**C**) in ligature-induced PD mice and ligature-induced PD mice treated with EVs, anti-CD80-EVs and anti-CD80-MTX-EVs. (**D**) Representative flow plots of $CD4^+$ $Foxp3^+$ cells populations in ligature-induced PD mice and ligature-induced PD mice treated with EVs, anti-CD80-EVs and anti-CD80-MTX -EVs. (**E-F**) Histogram of $CD4^+$ $Foxp3^+$ cells populations in gingival tissue (**E**) and cLN (**F**) in ligature-induced PD mice and ligature-induced PD mice treated with EVs, anti-CD80-EVs and anti-CD80-MTX-EVs. (**G**) Representative flow plots of $CD4^+$ IL-10^+ cells populations in ligature-induced PD mice and ligature-induced PD mice treated with EVs, anti-CD80-EVs and anti-CD80-MTX-EVs. (**H-I**) Histogram of $CD4^+$ IL-10^+ cells populations in gingival tissue (**H**) and cLN (**I**) in ligature-induced PD mice and ligature-induced PD mice treated with EVs, anti-CD80-EVs and anti-CD80-MTX-EVs. (**J**) Representative flow plots of $CD4^+$ T-bet^+ cells populations in ligature-induced PD mice and ligature-induced PD mice treated with EVs, anti-CD80-EVs and anti-CD80-MTX-EVs. (**K-L**) (**K**) and cLN (**L**) in ligature-induced PD mice and ligature-induced PD mice treated with EVs, anti-CD80-EVs and anti-CD80-MTX-EVs. (n ≥ 5, ns, not significant, *P < 0.05, **P < 0.01, ***P < 0.001, ****P < 0.0001).

https://doi.org/10.2147/IJN.S517357

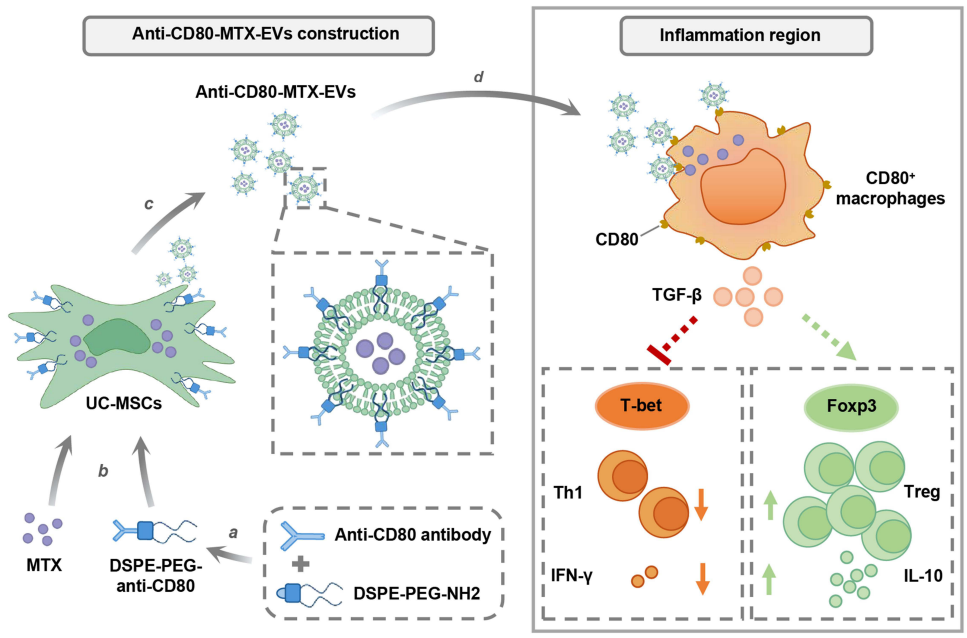

Figure 8 Schematic representation of the construction for anti-CD80-MTX-EVs, which target CD80$^+$ macrophages and deliver MTX to change their immune response. Anti-CD80-MTX-EVs treatment elevated TGF-β of macrophages, which promoted the production of Treg cells and reduced the proportion of Th1 cells, to resolve inflammation and induce homeostasis at the site of inflammation.

(Figure 8). Consequently, these findings demonstrate a novel therapeutic strategy for treating inflammatory diseases associated with excessive immune activation triggered by both exogenous and endogenous antigen stimulation.

Macrophages are very important in inflammatory diseases such as RA and PD.[30] Pro-inflammatory macrophages activate T cells to participate in adaptive immunity. Research has shown that the upregulation of IRF5 (interferon-regulatory factor 5) in pro-inflammatory macrophages was crucial for inducing cytokines (IL-12, IL-23 and TNF-α), which were involved in triggering Th1 and Th17 responses.[31] Additionally, activated macrophages secrete IL-12 and IL-23, they further affect the polarization of Th1 and Th17 cells.[32] Therefore, targeting macrophages and modulating their pro-inflammatory status are vital for immune regulation. Currently used methods for regulating macrophage functions include the addition of small molecule compounds, virus transfection, chemical synthesis material treatment, etc.[33] Nevertheless, these approaches suffer from certain limitations, including a poor targeting ability, elevated expenses, and concerns over biological security.[34] Stem cell-derived EVs, notably those from mesenchymal stem cells, have garnered considerable research attention in immunotherapeutic applications due to their low immunogenic potential and their notable immunomodulatory and anti-inflammatory effects.[16,35,36] However, the clinical application of EVs encounters obstacles such as the inefficient targeting of inflamed regions and inconsistent content profiles.[14]

Various research projects have explored the use of EVs in RA and PD.[37–39] Studies indicated that apoEVs originating from macrophages contribute to the resolution of synovitis through the induction of macrophage anti-inflammatory activation, thereby helping to restore the overall microenvironment homeostasis of rheumatoid arthritis joints.[40] However, due to the lack of targeted functionality in macrophage-apoEVs, their anti-inflammatory function may be limited. In response to this concern, our study focused on the significant increase of CD80$^+$ macrophages in the inflammatory site associated with CIA and experimental periodontitis. CD80 serves as a typical biomarker of pro-inflammatory macrophages. Therefore, anti-CD80-MTX-EVs could potentially act on a larger subset of pro-inflammatory macrophages with more potent functions. Consequently, we modified the surface of EVs with DSPE-PEG-anti-CD80 to endow them with the ability to target pro-inflammatory macrophages. In vivo and in vitro studies both demonstrated that incorporating DSPE-PEG-anti-CD80 greatly enhanced the efficiency of EVs binding to pro-inflammatory macrophages and effectively reduced CD80 expression of macrophages. On the basis of the targeting properties of anti-CD80-EVs, we

constructed a drug delivery system capable of transferring functional molecules utilizing the double-layer membrane structure present within EVs.

MTX, recognized as an immunosuppressant, is extensively employed for managing rheumatic conditions. Studies have established that MTX can potently reduce bone loss linked to arthritis[41] and acts as a probable modulator of macrophage polarization.[42] However, the overuse of MTX can result in severe adverse reactions, including harm to the oral and gastrointestinal mucosa, as well as liver and kidney impairments, thereby complicating the drug's therapeutic benefits and its broader use.[43] In this study, we obtained MTX-EVs by incorporating MTX into the culture system of hUCMSCs, aiming to mitigate the side effects of MTX while improving its therapeutic effect through encapsulation within EVs. Our experimental data demonstrated that compared to anti-CD80-EVs, anti-CD80-MTX-EVs had a further increased efficacy in reducing CD80 expression of macrophages, leading to significant alleviation of arthritis and periodontitis. Therefore, these engineered EVs with targeted drug delivery hold promise for precise, effective, and safe regulation of inflammatory macrophages.

Macrophages modulate immune homeostasis through TGF-β secretion across diverse physiological and pathological contexts.[44] During anti-inflammatory responses, macrophages release TGF-β following phagocytosis of apoptotic cells, effectively suppressing pro-inflammatory mediators (TNF-α, IL-6) to preserve a tissue-reparative microenvironment.[45–48] It is noteworthy that in the present study, the novel drug delivery system we developed not only reduced CD80 expression in macrophages but also effectively elevated TGF-β levels. RNA-seq analysis demonstrated a significant upregulation of TGF-β-related genes in macrophages following MTX-EVs treatment. Furthermore, ELISA assays revealed a substantial increase in TGF-β protein levels in macrophages treated with MTX-EVs in vitro. This phenomenon may be closely associated with the establishment of an anti-inflammatory immune microenvironment. Moreover, TGF-β is a pivotal cytokine for the induction of Treg cell generation.[49] Our study demonstrated that TGF-related genes in macrophage were significantly upregulated following MTX-EVs treatment, as evidenced by RNA-seq analysis of treated macrophages. Furthermore, both in vitro PCR and ELISA assays consistently revealed substantial increases in TGF-β-related genes and TGF-β protein levels. IFN γ is predominantly secreted by activated Th1 lymphocytes, playing a pivotal role in orchestrating adaptive immune responses.[50] In contrast, IL-10 is primarily synthesized by regulatory T cells (Tregs), functioning to suppress pro-inflammatory mediators (including TNF-α and IL-6) and attenuate MHC class II molecule expression on antigen-presenting cells (APCs), thereby limiting excessive inflammatory responses while preserving immune tolerance.[51,52] Through various experimental approaches, we further confirmed that anti-CD80-MTX-EVs treatment significantly elevated the proportion of IL-10$^+$ T cells and IL-10 concentration in inflamed tissues, while simultaneously reducing the proportion of Th1 cells and IFN γ levels. These findings collectively indicate that anti-CD80-MTX-EVs drive a systemic shift in the immune microenvironment from hyperinflammation toward inflammation resolution. In conclusion, the findings further underscore the remarkable efficacy and broad utility of anti-CD80-MTX-EVs for addressing inflammatory conditions.

While anti-CD80-MTX-EVs show great potential as therapeutic agents for inflammatory conditions, numerous obstacles must be addressed in the transition from laboratory research to clinical application. Firstly, standardized procedures of quantity production and quality control methods need to be clearly defined.[53] In addition, the details of pharmacokinetics and pharmacodynamic processes in the application of anti-CD80-MTX-EVs remain to be explored for clinical application.[54] Importantly, in addition to macrophages, dendritic cells[55] and B lymphocytes[56] can also express CD80. The regulatory effects of our engineered vesicles on these specific cell populations warrant further investigation in subsequent studies.

Conclusion

In this study, we successfully constructed engineered vesicles capable of targeting inflammatory macrophages for MTX delivery, which promote the TGF-β secretion of macrophages, and induce the generation of Treg cells. Moreover, anti-CD80-MTX-EVs significantly alleviated rheumatoid arthritis and periodontitis by reducing CD80$^+$ macrophages, promoting the proportion of Treg cells and inhibiting the generation of Th1. In conclusion, although considerable advancements are still needed for its application in clinical settings, the anti-CD80-MTX-EVs show potential in contributing to the understanding of targeted drug delivery and effective management of inflammatory diseases.

Ethics

All experimental procedures involving animals were given by the Animal Protection Committee of the Fourth Military Medical University (IACUC-20230150). All procedures were in compliance with the relevant guidelines and regulations. Animal welfare and experimental procedures were complied with the principles of Laboratory Animal-Guidelines for ethical review of animal welfare (GB/T 35892-2018). The human umbilical cord mesenchymal stem cells (hUCMSCs) were obtained with informed donor consent following healthy births from Tangdu Hospital. All processes were approved and supervised by the Ethics Committee of Tangdu Hospital of the Fourth Military Medical University and followed the Declaration of Helsinki.

Acknowledgments

We extend our gratitude to all members of the Center for Tissue Engineering for their insightful discussions and critical review of the manuscript. This research was supported by grants from the National Key Research and Development Program of China (2021YFA1100600), the National Natural Science Foundation of China (82370927), and the Shaanxi Provincial Key Research and Development Program (2023-ZDLSF-49).

Disclosure

The authors report no potential conflicts of interest in this work.

References

1. Karin M, Clevers H. Reparative inflammation takes charge of tissue regeneration. *Nature*. 2016;529:307–315. doi:10.1038/nature17039
2. Schett G, Neurath MF. Resolution of chronic inflammatory disease: universal and tissue-specific concepts. *Nat Commun*. 2018;9:3261. doi:10.1038/s41467-018-05800-6
3. Gray JI, Farber DL. Tissue-resident immune cells in humans. *Annu Rev Immunol*. 2022;40:195–220. doi:10.1146/annurev-immunol-093019-112809
4. Redlich K, Smolen JS. Inflammatory bone loss: pathogenesis and therapeutic intervention. *Nat Rev Drug Discov*. 2012;11:234–250. doi:10.1038/nrd3669
5. Orecchioni M, Ghosheh Y, Pramod AB, et al. Macrophage polarization: different gene signatures in M1(LPS+) vs. classically and M2(LPS-) vs. alternatively activated macrophages. *Front Immunol*. 2019;10:1084. doi:10.3389/fimmu.2019.01084
6. Arnold CE, Gordon P, Barker RN, et al. The activation status of human macrophages presenting antigen determines the efficiency of Th17 responses. *Immunobiology*. 2015;220(1):10–19. doi:10.1016/j.imbio.2014.09.022
7. Muntjewerff EM, Meesters LD, van den Bogaart G. Antigen cross-presentation by macrophages. *Front Immunol*. 2020;11:1276. doi:10.3389/fimmu.2020.01276
8. Tang-Huau TL, Gueguen P, Gou Dot C, et al. Human in vivo-generated monocyte-derived dendritic cells and macrophages cross-present antigens through a vacuolar pathway. *Nat Commun*. 2018;9:2570. doi:10.1038/s41467-018-04985-0
9. Bittner S, Hehlgans T, Feuerer M. Engineered Treg cells as putative therapeutics against inflammatory diseases and beyond. *Trends immunol*. 2023;44:468–483. doi:10.1016/j.it.2023.04.005
10. Sakaguchi S, Yamaguchi T, Nomura T, et al. Regulatory T cells and immune tolerance. *Cell*. 2008;133:775–787. doi:10.1016/j.cell.2008.05.009
11. Coleman MM, Ruane D, Moran B, et al. Alveolar macrophages contribute to respiratory tolerance by inducing FoxP3 expression in naive T cells. *Am J Respir Cell Mol Biol*. 2013;48(6):773–780. doi:10.1165/rcmb.2012-0263OC
12. Allard B, Panariti A, Martin JG. Alveolar macrophages in the resolution of inflammation, tissue repair, and tolerance to infection. *Front Immunol*. 2018;9:1777. doi:10.3389/fimmu.2018.01777
13. Soroosh P, Doherty TA, Duan W, et al. Lung-resident tissue macrophages generate Foxp3+ regulatory T cells and promote airway tolerance. *J Exp Med*. 2013;210:775–788. doi:10.1084/jem.20121849
14. Richter M, Vader P, Fuhrmann G. Approaches to surface engineering of extracellular vesicles. *Adv Drug Delivery Rev*. 2021;173:416–426. doi:10.1016/j.addr.2021.03.020
15. Skotland T, Iversen TG, Llorente A, et al. Biodistribution, pharmacokinetics and excretion studies of intravenously injected nanoparticles and extracellular vesicles: possibilities and challenges. *Adv Drug Delivery Rev*. 2022;186:114326. doi:10.1016/j.addr.2022.114326
16. Manchon E, Hirt N, Bouaziz JD, et al. Stem cells-derived extracellular vesicles: potential therapeutics for wound healing in chronic inflammatory skin diseases. *Int J Mol Sci*. 2021;22:3130. doi:10.3390/ijms22063130
17. Zheng J, Kong Y, Hu X, et al. MicroRNA-enriched small extracellular vesicles possess odonto-immunomodulatory properties for modulating the immune response of macrophages and promoting odontogenesis. *Stem Cell Res Ther*. 2020;11:517. doi:10.1186/s13287-020-02039-1
18. Kalluri R, McAndrews KM. The role of extracellular vesicles in cancer. *Cell*. 2023;186:1610–1626. doi:10.1016/j.cell.2023.03.010
19. Su N, Hao Y, Wang F, et al. Mesenchymal stromal exosome-functionalized scaffolds induce innate and adaptive immunomodulatory responses toward tissue repair. *Sci Adv*. 2021;7:eabf7207. doi:10.1126/sciadv.abf7207
20. Tang TT, Wang B, Wu M, et al. Extracellular vesicle-encapsulated IL-10 as novel nanotherapeutics against ischemic AKI. *Sci Adv*. 2020;6:eaaz0748. doi:10.1126/sciadv.aaz0748
21. Wang W, Zhou H, L L. Side effects of methotrexate therapy for rheumatoid arthritis: a systematic review. *Eur J Med Chem*. 2018;158:502–516. doi:10.1016/j.ejmech.2018.09.027
22. Solomon DH, Glynn RJ, Karlson EW, et al. Side effects of low-dose methotrexate. A*nnals of internal medicine*. 2020; 172: 369.

23. Cronstein BN, Aune TM. Methotrexate and its mechanisms of action in inflammatory arthritis. *Nat Rev Rheumatol*. 2020;16:145–154. doi:10.1038/s41584-020-0373-9
24. Ye Z, Zhang T, He W, et al. Methotrexate-loaded extracellular vesicles functionalized with therapeutic and targeted peptides for the treatment of glioblastoma multiforme. *ACS Appl Mater Interfaces*. 2018;10:12341–12350. doi:10.1021/acsami.7b18135
25. Guo M, Wu F, Hu G, et al. Autologous tumor cell-derived microparticle-based targeted chemotherapy in lung cancer patients with malignant pleural effusion. *Sci Transl Med*. 2019;11:1.
26. Tardito S, Martinelli G, Soldano S, et al. Macrophage M1/M2 polarization and rheumatoid arthritis: a systematic review. *Autoimmunity Rev*. 2019;18:102397. doi:10.1016/j.autrev.2019.102397
27. Kurowska-Stolarska M, Alivernini S. Synovial tissue macrophages in joint homeostasis, rheumatoid arthritis and disease remission. *Nat Rev Rheumatol*. 2022;18:384–397. doi:10.1038/s41584-022-00790-8
28. He XT, Li X, Zhang M, et al. Role of molybdenum in material immunomodulation and periodontal wound healing: targeting immunometabolism and mitochondrial function for macrophage modulation. *Biomaterials*. 2022;283:121439. doi:10.1016/j.biomaterials.2022.121439
29. Hajishengallis G, George Hajishengallis. Immunology, Periodontitis: from microbial immune subversion to systemic inflammation. *Nat Rev Immunol*. 2015;15(1):30–44. doi:10.1038/nri3785
30. Liu H, Chen Y, Huang Y, et al. Macrophage-derived mir-100-5p orchestrates synovial proliferation and inflammation in rheumatoid arthritis through mTOR signaling. *J Nanobiotechnol*. 2024;22:197. doi:10.1186/s12951-024-02444-1
31. Krausgruber T, Blazek K, Smallie T, et al. IRF5 promotes inflammatory macrophage polarization and TH1-TH17 responses. *Nat Immunol*. 2011;12:231–238. doi:10.1038/ni.1990
32. Davies LC, Jenkins SJ, Allen JE, et al. Tissue-resident macrophages. *Nat Immunol*. 2013;14(10):986–995. doi:10.1038/ni.2705
33. Peng J, Li J, Huang J, et al. p300/CBP inhibitor A-485 alleviates acute liver injury by regulating macrophage activation and polarization. *Theranostics*. 2019;9:8344–8361. doi:10.7150/thno.30707
34. Shayman JA, Larsen SD. The development and use of small molecule inhibitors of glycosphingolipid metabolism for lysosomal storage diseases. *J Lipid Res*. 2014;55:1215–1225. doi:10.1194/jlr.R047167
35. Deun JV, Mestdagh P, Sormunen R, et al. The impact of disparate isolation methods for extracellular vesicles on downstream RNA profiling. *J Extracell Vesicles*. 2014;3:1.
36. Takeda M, Akamatsu S, Kita Y, et al. Nanomaterials, the roles of extracellular vesicles in the progression of renal cell carcinoma and their potential for future clinical application. *Nanomaterials*. 2023;13(10):1611. doi:10.3390/nano13101611
37. Lin M, Lei S, Chai Y, et al. Immunosuppressive microvesicles-mimetic derived from tolerant dendritic cells to target T-lymphocytes for inflammation diseases therapy. *Nanobiotechnology*. 2024;22:201. doi:10.1186/s12951-024-02470-z
38. Takenaka M, Yabuta A, Takahashi Y, et al. Interleukin-4-carrying small extracellular vesicles with a high potential as anti-inflammatory therapeutics based on modulation of macrophage function. *Biomaterials*. 2021;278:121160. doi:10.1016/j.biomaterials.2021.121160
39. Chen J, Shi X, Deng Y, et al. miRNA-148a-containing GMSC-derived EVs modulate Treg/Th17 balance via IKKB/NF-κB pathway and treat a rheumatoid arthritis model. *JCI Insight*. 2024;9. doi:10.1172/jci.insight.177841
40. Li X, Li S, Fu X, et al. Apoptotic extracellular vesicles restore homeostasis of the articular microenvironment for the treatment of rheumatoid arthritis. *Bioact Mater*. 2024;35:564–576. doi:10.1016/j.bioactmat.2023.11.019
41. Bluett J, Riba-Garcia I, Verstappen SMM, et al. Development and validation of a methotrexate adherence assay. *Ann Rheumatic Dis*. 2019;78:1192–1197. doi:10.1136/annrheumdis-2019-215446
42. D. Arruda JAA, Corrêa JD, Singh Y, et al. Methotrexate promotes recovery of arthritis-induced alveolar bone loss and modifies the composition of the oral-gut microbiota. *Silva Anaerobe*. 2022;75:102577. doi:10.1016/j.anaerobe.2022.102577
43. Guo L, Chen Y, Wang T, et al. Rational design of metal-organic frameworks to deliver methotrexate for targeted rheumatoid arthritis therapy. *J Control Release*. 2021;330:119–131. doi:10.1016/j.jconrel.2020.10.069
44. Xu Y, Ying L, Lang JK, et al. Modeling mechanical activation of macrophages during pulmonary fibrogenesis for targeted anti-fibrosis therapy. *Sci Adv*. 2024;10(13):eadj9559. doi:10.1126/sciadv.adj9559
45. Striz I, Brabcova E, Kolesar L, et al. Cytokine networking of innate immunity cells: a potential target of therapy. *Clin Sci*. 2014;126(9):593–612. doi:10.1042/CS20130497
46. Branchett WJ, Lloyd CM. Regulatory cytokine function in the respiratory tract. *Mucos immunol*. 2019;12(3):589–600. doi:10.1038/s41385-019-0158-0
47. Hasegawa Y, Daigo hashimoto ZZ, Zhang Z, et al. GVHD targets organoid-forming bile duct stem cells in a TGF-β-dependent manner. *Blood*. 2024;144(8):904–913. doi:10.1182/blood.2023023060
48. Sanjabi S, Oh SA, Li MO. Regulation of the immune response by TGF-β: from conception to autoimmunity and infection. *Cold Spring Harbor Perspect Biol*. 2017;9(6):a022236. doi:10.1101/cshperspect.a022236
49. Travis MA, Sheppard D. TGF-β activation and function in immunity. *Ann Rev Immunol*. 2014;32:51–82. doi:10.1146/annurev-immunol-032713-120257
50. Ivashkiv LB. IFNγ: signalling, epigenetics and roles in immunity, metabolism, disease and cancer immunotherapy. *Nat Rev Immunol*. 2018;18(9):545–558. doi:10.1038/s41577-018-0029-z
51. Saxton RA, Tsutsumi N, Su LL, et al. Structure-based decoupling of the pro- and anti-inflammatory functions of interleukin-10. *Science*. 2021;371(6535). doi:10.1126/science.abc8433.
52. Rubtsov YP, Rasmussen JP, Chi EY, et al. Regulatory T cell-derived interleukin-10 limits inflammation at environmental interfaces. *Immunity*. 2008;28(4):546–558. doi:10.1016/j.immuni.2008.02.017
53. Agrahari V, Agrahari V, Burnouf PA, et al. Extracellular microvesicles as new industrial therapeutic frontiers. *Trends Biotechnol*. 2019;37:707–729. doi:10.1016/j.tibtech.2018.11.012
54. Wiklander OPB, Brennan MÁ, Lötvall J, et al. Advances in therapeutic applications of extracellular vesicles. *Sci trans med*. 2019;11:eaav8521. doi:10.1126/scitranslmed.aav8521
55. Cui B, Sun J, Li S, et al. CD80+ dendritic cell derived exosomes inhibit CD8+ T cells through down-regulating NLRP3 expression after liver transplantation. *Int Immunopharmacol*. 2022;109:108787. doi:10.1016/j.intimp.2022.108787
56. Lorenzetti R, Janowska I, Roberto Smulski C, et al. Abatacept modulates CD80 and CD86 expression and memory formation in human B-cells. *J Autoimmun*. 2019;101:145–152. doi:10.1016/j.jaut.2019.04.016